Journal of Network Intelligence
Taiwan Ubiquitous Information
 ISSN 2414-8105
Volume **9**, Number **4**, November **2024**

3D Human Animation Design based on Fusion Generation of Adversarial Networks and B-Spline Differences

Li Cheng

Department of Creative Studies,
Changzhou Vocational Institute of Textile and Garment, Changzhou 213164, China
lcheng@cztgi.edu.cn

Hao Su

Department of Creative Studies,
Changzhou Vocational Institute of Textile and Garment, Changzhou 213164, China
hsu@cztgi.edu.cn

Ru-Jing Yao*

Academy of Art and Design
Anhui University of Technology, Ma'anshan 243002, China
lomoyao@126.com

*Corresponding author: Ru-Jing Yao
Received October 10, 2023, revised January 7, 2024, accepted April 29, 2024.

Abstract. *To meet the social demand for the design details and accuracy of 3-dimensional human animation, the reconstruction algorithm based on B spline is constructed to improve the smoothness and fidelity of the traditional model. In addition, the study uses generative adversarial networks to build back texture generation algorithms to solve the missing information in traditional models. Finally, the 3-dimensional body animation design method is constructed based on the modified human model reconstruction algorithm and the back texture generation algorithm. The improved algorithm is empirically analyzed. The average fitting error of the human body model reconstruction algorithm is 4.6*10-4. The average fit error is 3.2*10-4 lower than the traditional splicing-fusion algorithm, which is 0.8*10-4 smaller than the T-spline algorithm, and 1.2*10-4 smaller than the splice algorithm based on T-spline value. The improved algorithm for back texture generation has a peak signal-to-noise ratio of 25.6 dB, which is 1.8dB higher than the back texture generation algorithm based on variational auto-encoder and 9.6dB higher than the back texture generation algorithm based on auto-encoder. The quality of the generated images is higher than the comparison algorithm. In addition, performance comparison experiments are conducted on the 3-dimensional human animation design method based on B-spline difference and generative adversarial network. The action matching accuracy of this method is 87.8%, which can meet the requirements of correct matching of 3-dimensional animation action. Based on the above results, the 3-dimensional human animation method can meet the social needs and improve the quality and authenticity of animation generation.*
Keywords: generative adversarial network; b-spline difference; 3D human body model; animation design; back texture generation

1. **Introduction.** In recent years, with the rapid development of computer graphics and computer vision, human animation design has become a highly focused research field. The goal of human animation design is to simulate and present the actions and expressions of human bodies, making them more realistic in virtual environments [1, 2]. Realistic human animation can improve the immersion, interaction and visual effects in the virtual environment, expanding the application field of human animation. This is important for improving the user experience, creating more attractive virtual scenes, and meeting the needs of game development, movie production, virtual reality, and architecture and industrial design [3]. However, due to the complexity and diversity of human movements, and the requirements for animation details, traditional animation design methods are prone to problems, including unnatural human form, incoherent movements and low generation quality. Therefore, to realize high-quality human animation design, the study proposes functional improvement in traditional animation design to improve the authenticity and quality of human animation generation. B-spline difference is a commonly used method for curve and surface reconstruction, which has good smoothness and approximation. Based on a large amount of collected human body data, high-precision human body models can be obtained through B-spline difference processing [4]. The Generative Adversarial Network (GAN) is a machine algorithm composed of generators and discriminators, which has wide applications in realistic image generation and conversion. However, currently, research on GAN for solving 3D human animation design is limited [5, 6]. Based on this, B-spline difference is used to reconstruct a 3D human model and infer the complete back texture through GAN, thereby achieving more realistic and vivid human animation design. The research can be used in game development, film making, virtual and augmented reality, and architectural and industrial design, providing higher quality, more realistic and smoother human animation effects. It can also improve user experience, enhance visual and emotional experience, and improve production efficiency and quality.

The first section elaborates on the current development status of B-spline difference, GAN, and 3D animation. The second section constructs a human model reconstruction algorithm based on B-spline difference. Then the back texture generation algorithm based on GAN and the 3D human animation synthesis method based on B-spline difference and GAN are constructed. In the third section, empirical analysis is conducted on the proposed human model reconstruction algorithm, GAN back texture generation algorithm, and 3D human animation synthesis method based on B-spline difference and GAN. The fourth section is the conclusion and future research directions.

1.1. **Related Work.** The traditional 3D human animation methods mainly include manual modeling, key-frame animation and motion capture techniques. Manual modeling requires high modeling skills and experience for modeling teachers. It is also time-consuming and prone to unnatural action effects. Key-frame animation requires the animator to manually set key-frames and adjust curves, but requires a lot of time and effort for complex human movements. Motion capture technology can provide highly realistic motion effects, but requires a large amount of equipment and venues. There may be inaccurate or missing data for complex movements and scenarios. Therefore, new methods need to be developed to improve the fidelity and fluency of 3 D human animation to meet the needs of animation production.

B spline interpolation is a mathematical method for curve and surface fitting, which can be used to realize curve and surface dynamics in animations. GAN is a machine learning model that can generate more realistic data through constant adversarial and learning. GAN is widely used in image generation and video generation. When B spline interpolation and GAN are combined and applied to 3D animation, smooth animation

curves and surfaces can be generated based on B spline interpolation. Then more realistic and smooth animation content is generated by GAN. The latest progresses of B spline interpolation, GAN and 3D animation are as follows.

(1) With the rapid development of computer technology, B-spline difference and GAN are widely used in various fields. To improve the numerical simulation accuracy of significant deformation problems, Sun et al. [7] constructed a large deformation solid mechanics calculation method using high-order continuous B-spline difference. Through effectiveness analysis, it significantly improves the simulation accuracy and convergence of significant deformation solid mechanics problems compared to traditional methods. To expand the Chebyshev space and dimensions, Hiemstra et al. [8] constructed a B-spline basis method using matrices. The expansion efficiency and reliability of this method are superior to the classical B-spline basis method, which has practical application value. To address the detail loss in super-resolution reconstructed images, Zhu et al. [9] utilized GAN to construct an improved single image super-resolution reconstruction method. The generated super-resolution image peak signal-to-noise ratio (PSNR) and structural similarity visual effects of this method are superior to other comparison methods. Its image reconstruction performance exceeds other comparison methods, which has practical application value. In the map construction model of remote sensing images, land surface observations are affected by cloud light transmission and scattering. Chen et al. [10] proposed a thin cloud removal method for land surface observation based on GAN. Empirical analysis shows that this method performs better than other comparative methods in restoring texture of remote sensing images. It can be applied in practical image rendering.

(2) With the further deepening of computer technology research, its application in 3D animation design research is also increasing. To meet the understanding needs of crystallographic concepts, Aristov et al. [11] used Blender to construct a 3D model library of crystallography. This model library can assist users in learning crystallographic concepts, quickly understanding abstract crystallographic concepts and meeting educational needs. To assist surgeons in making quick anatomical decisions during cervical mediastinal lymph node resection, Ishida et al. [12] proposed a 3D CG animation based on Light-Wave for cervical upper mediastinal esophageal dissection. The 3D CG animation has high quality, which is similar to real surgery. It can provide auxiliary support for clinical doctors in actual cervical upper mediastinal esophageal dissection surgery. The concepts related to metabolism in biochemistry and life sciences are highly abstract and difficult for students to understand. Therefore, Long et al. [13] utilized 3D animation to introduce metabolic related concepts. This method improves learning engagement and enhances students' confidence in understanding concepts, which has practical application value. To improve the efficiency of animation production, Dvoroňák et al. [14] constructed an animation production method using 3D inflation and a novel rigid protection layered deformation model. The performance and effectiveness of this method are verified. Compared to traditional methods, it has better production efficiency and effectiveness. This can improve the efficiency of animation production.

(3) To address the different challenging tasks of complex pose accuracy in robotics, human-computer interaction, and character animation, Sebastian et al. [15] proposed a new rapid etiology evolution algorithm. The validity of the algorithm can be solved with multiple end actuators and target complete constraint general inverse kinematics. It can be used for Unity3D and robot operating system. To optimize the shape adaptation of the grid in the animation or deformation, Zhou et al. [16] proposed a quadrilateral mesh scheme that utilizes the one-to-one relationship of oil pumps to generate non rigid objects. The effectiveness of the scheme is verified. The model can effectively avoid the under sampling problem of the grid and reduce artifacts effectively. To improve the

diagnostic efficiency of medical rehabilitation patients, ACS JD et al. [17] proposed a projection animation method based on virtual technology. From the results, the method can scan the facial and oral patients. Combined with relevant information, a noninvasive and reliable diagnostic method is provided for clinical results prediction. To improve the learning interest, Singla et al. [18] constructed a cell environment animation method based on tetrahedral structural blocks. An empirical experiment is conducted on the animation. The results show that teachers and students are highly satisfied with the educational animation, which can improve students' understanding for cell characteristics and function information.

1.2. **Motivation and contribution.** From the above analysis, the combination of GAN and B spline interpolation can generate high-quality animation while ensuring the fluency and authenticity of human body animation.

Therefore, to effectively improve the quality of human animation, this work based on skeleton driven parametric human parkin (Skinned Multi-Person Linear eXpressive, SMPL-X), B spline difference and the back texture generation algorithm based on GAN, achieving high-quality 3D human body animation design. The human model reconstruction algorithm and human model reconstruction algorithm steps are introduced in detail. The method is tested and the corresponding experimental results are compared. The main innovations and contributions of this work are as follows.

(1) The GAN is used to generate human models with realistic appearance and movement characteristics. The integrating B spline difference technology is used to smooth the action of the manikin, making it more natural and smooth, and improving the fidelity of the body animation.

(2) The GAN and B spline difference can automatically generate a realistic human body animation, saving the production time and cost. Then it is also improves the efficiency and quality of animation production, and expands its application field. In virtual reality and game development. A realistic character animation can be created more quickly to improve user experience.

2. 3D human animation design based on fusion generative adversarial network and B-Spline differences.

2.1. **Improved human model reconstruction algorithm based on B-Spline difference.** Skinned Multi-Person Linear eXpressive (SMPL-X), B-spline difference, and GAN based back texture generation algorithm are designed to achieve high-quality 3D human animation design. With the development of technology, the requirements for the fidelity and authenticity of human models are becoming increasing. The SPML-X model is used to extract parameters from the 3D human body information of the input image, generating a 3D human body model with both sides. In addition, to further improve the realism and accuracy of the model, a model stitching and fusion algorithm based on B-spline difference is studied to complete the replacement and fusion of each model. The human model reconstruction algorithm based on B-spline difference proposed in the research is shown in Figure 1.

In Figure 1, the proposed improved human model reconstruction algorithm based on B-spline difference can be divided into two parts. They are human generated models based on SMPL-X, as well as model stitching and fusion based on B-spline differences. In the generation of human body models based on SMPL-X, firstly, posture parameters, morphological parameters, and expression parameters are extracted from human body images to obtain 3D human body front and back models. Then, the hand geometry of the model is cropped based on joint points to obtain the boundary point data set. The

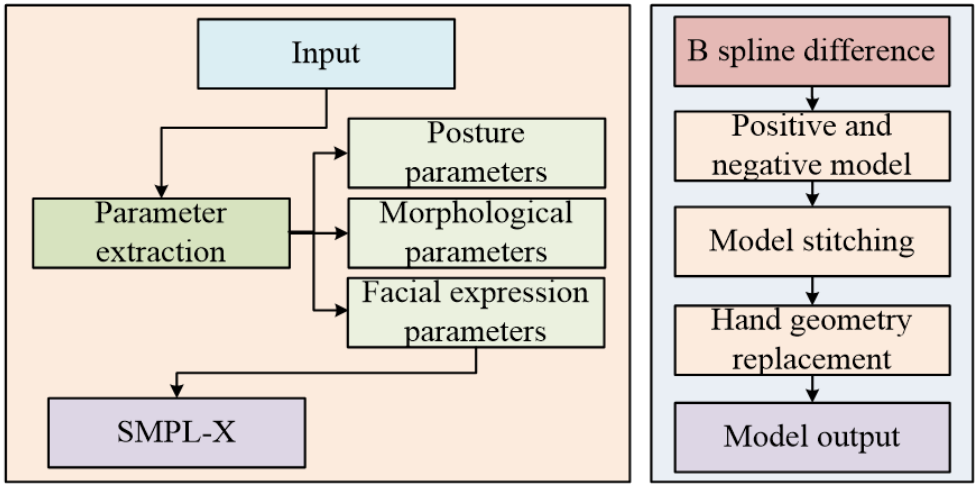

Figure 1. Modified human model reconstruction algorithm

hand data is combined with the human body 3D model data. The boundary points are matched and concatenated using a B-spline difference based stitching fusion algorithm. A realistic human body parameterized model reconstruction is completed. The SMPL-X model is shown in Figure 2.

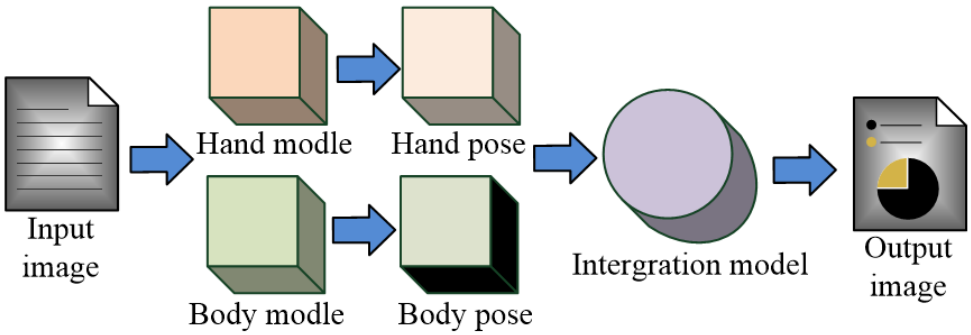

Figure 2. The SMPL-X model

The SMPL-X model uses a hybrid deformation algorithm based on vertex linear hybrid skin, which can express human actions and emotions. The vertex set of the SMPL-X model is shown in Formula (1).

$$\begin{cases} M(\overrightarrow{\theta}, \overrightarrow{\beta}, \overrightarrow{\psi}, \phi) : \mathbb{R}^{|\overrightarrow{\theta}|\times|\overrightarrow{\beta}|\times|\overrightarrow{\psi}|} \to \mathbb{R}^{3N} \\ \phi = \{\overline{T}, W, S, J, P, E\} \end{cases} \tag{1}$$

In Formula (1), M represents the vertex set of the SMPL-X model. $\overrightarrow{\theta}$ represents the pose control parameter, $\overrightarrow{\beta}$ represents the shape control parameter, $\overrightarrow{\psi}$ represents the expression control parameter, and ϕ represents the known parameters after training. $\overline{T}$ represents the initial set of fixed points, W represents the mixed weights after training, S represents the orthogonal principal component of human body shape deviation, J represents the transformation matrix between vertices and human joint points, P represents the pose offset matrix, and E represents the principal component of facial expression changes. The vertex set of the SMPL-X model is transformed, as shown in Formula (2).

$$\begin{cases} M(\overrightarrow{\theta}, \overrightarrow{\beta}, \overrightarrow{\psi}; \phi) \Rightarrow M(\overrightarrow{\theta}, \overrightarrow{\beta}, \overrightarrow{\psi}) = F(T_p(\overrightarrow{\theta}, \overrightarrow{\beta}, \overrightarrow{\psi}), \overrightarrow{\theta}, \overrightarrow{\beta}, \overrightarrow{\psi}, W) \\ T_p(\overrightarrow{\theta}, \overrightarrow{\beta}, \overrightarrow{\psi}) = \overline{T} + B_s(\overrightarrow{\beta}) + B_p(\overrightarrow{\theta}) + B_E(\overrightarrow{\psi}) \end{cases} \tag{2}$$

In Formula (2), $T_p(\overrightarrow{\theta}, \overrightarrow{\beta}, \overrightarrow{\psi})$ represents the set of vertex positions for the initial pose. $B_s(\overrightarrow{\beta})$ represents the vertex displacement caused by morphological parameters, $B_p(\overrightarrow{\theta})$ represents the vertex displacement caused by pose parameters, and $B_E(\overrightarrow{\psi})$ represents the morphological differences influenced by facial expression parameters. The mixed shape parameter of the expression is shown in Formula (3).

$$\begin{cases} B_E(\overrightarrow{\psi}; E) = \sum_{n=1}^{|\overrightarrow{\psi}|} \psi_n \epsilon_n \\ E = [\epsilon_1, \epsilon_2, \ldots, \epsilon_n], \quad n = 10 \end{cases} \tag{3}$$

In Formula (3), E represents the set of principal components for expression changes, and ϵ_n represents expression changes. At this point, the vertex position change of the SMPL-X model is shown in Formula (4).

$$\vec{t_i} = \sum_{k=1}^{K} W_{k,i} G_k(\overrightarrow{\theta}, J(\overrightarrow{\beta}))(t_i + b_{s,i}(\overrightarrow{\beta}) + b_{p,i}(\overrightarrow{\theta})) + b_{E,i}(\overrightarrow{\psi}) \tag{4}$$

In Formula (4), $b_{S,i}(\overrightarrow{\beta})$ represents the offset of vertex i in $b_S(\overrightarrow{\beta})$ caused by shape, posture, and facial expression parameters. $b_{S,i}(\overrightarrow{\beta})$ also includes the cumulative effect of these parameters on the vertex position. After constructing the front and back models of the human body, the models are spliced and fused. B-spline difference, a commonly used interpolation method, can describe complex shapes using only a small number of control vertices, enabling efficient reconstruction of human body data [15,16]. To enhance the authenticity and accuracy of the model, a human body model stitching and fusion algorithm is constructed based on B-spline differences. The implementation process of this algorithm is shown in Figure 3.

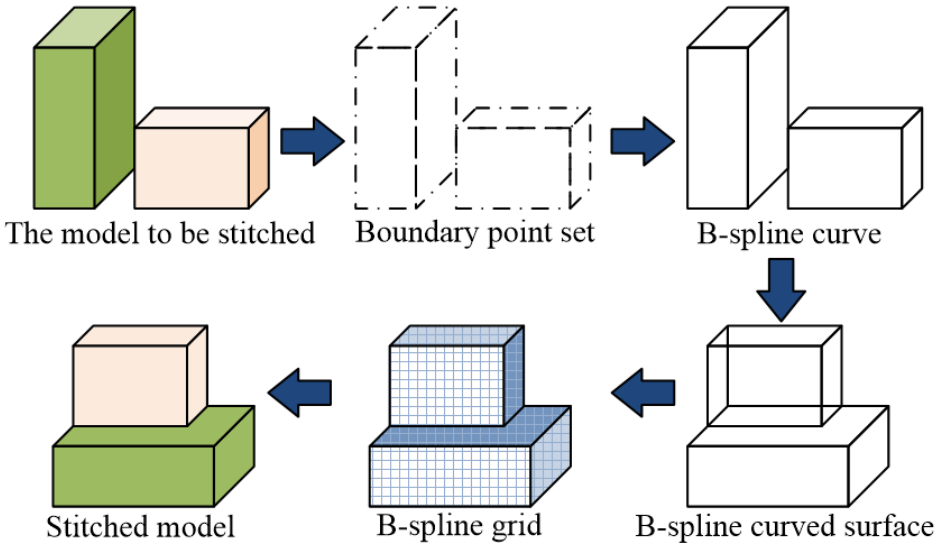

Figure 3. Implementation process of manikin splicing fusion algorithm

In Figure 3, firstly, the boundary point set of the model to be spliced is extracted for data. To ensure the smoothness and naturalness of model stitching and fusion, a model

stitching and fusion algorithm based on cubic B-spline difference is studied. Based on the boundary points, four cubic uniform B-spline curve is generated. Then the boundary vertices are collected, as shown in Formula (5).

$$P(u) = \sum_{i=0}^{n} P_i B_{i,k}(u), u = [u_{k-1}, u_{n+1}] \tag{5}$$

In Formula (5), u_i represents the node value. P_i is the control vertex. $B_{i,k}(u)$ represents the cardinality of k-th order N-splines. The recursive formula is shown in Formula (6).

$$\begin{cases} B_{i,k}(u) = \begin{cases} 1, u_i < u < u_{i+1} \\ 0, otherwise \end{cases} \\ B_{i,k}(u) = \frac{u-u_i}{u_{i+k-1}-u_i} B_{i,k-1}(u) + \frac{u_{i+k}-u}{u_{i+k-1}-u_i} B_{i+1,k-1}(u) \end{cases} \tag{6}$$

In Formula (6), the support interval of $B_{i,k}(u)$ is $[u_i, u_{i+k}]$. The definition interval of a B-spline curve is $[u_{k-1}, u_{n+1}]$. The control vertices on the B-spline are independent of each other. The influence interval is $[u_i, u_{i+k}]$. The spatial control point is $P_{i,j}$ $(i = 0, 1, 2, \ldots, m; j = 0, 1, 2, \ldots, n)$. Subsequently, the boundary vertices are used to inverse the control vertices of the B-spline curve. The node vector based on the parameter axis is used to define the B-spline surface. Then the cubic B-spline surface is constructed, as shown in Formula (7).

$$P(u, v) = \sum_{i=0}^{m} \sum_{j=0}^{n} P_{i,j} N_{i,p}(u) N_{j,q}(v); u \in [u_{p-1}, u_{m+1}], v \in [u_{q-1}, u_{n+1}] \tag{7}$$

In Formula (7), u and v represent the parameter axes of the B-spline difference. $P_{i,j}$ represents the control grid. $N_{i,p}(u)$ represents the basis of the B-spline derived from u based on the parameter axis. F represents the basis of the B-spline derived from v based on the parameter axis.

2.2. **Back texture generation algorithm based on adversarial generation network.** After constructing the human body 3D model, further refinement for human texture information is carried out on the basis of the 3D model. However, due to the occlusion of the input image, the input image generally has complete human body texture information on the front, but lacks human body texture information on the back. Due to the similarity of the front and back textures, it is feasible to derive the back texture information of the human body based on the front human texture information [19, 20]. GAN is a machine learning model composed of generators and discriminators, which is used to generate realistic data samples [21]. GAN is used to construct a back texture generation algorithm. This algorithm completes the back texture image output based on front texture derivation through training the generator and discriminator network. The basic structure of GAN is shown in Figure 4.

In Figure 4, the GAN structure includes two parts, a generator and a discriminator. The goal of the generator is to generate as realistic a sample as possible. A random noise vector z is received as input. By learning the feature distribution $P_{\text{data}}(x)$ of real data x, a false sample similar to the real sample is output. The probability distribution $P_z(x)$ and $P_{\text{data}}(x)$ of random noise z are fitted as much as possible. The generator can continuously optimize network parameters, so that the generated false samples can be judged by the discriminator. The goal of the discriminator is to distinguish difference between the false sample $G(z)$ generated by the generator and the real sample x. Like generators, discriminators can accurately distinguish between real and false samples by continuously optimizing network parameters. Therefore, the GAN training is a game

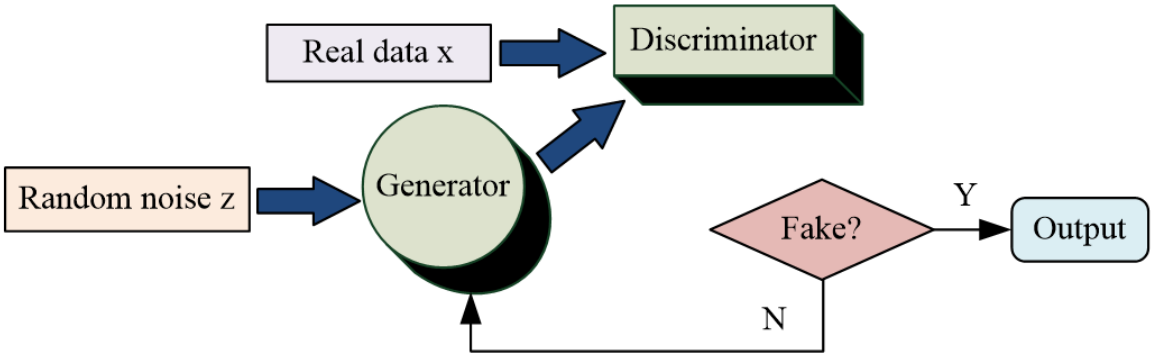

Figure 4. Basic structure of GAN

process. Generators and discriminators compete and influence each other. The loss function of the discriminator is shown in Formula (8).

$$\max_D V(D,G) = \mathbb{E}_{x\sim P_{\text{data}}(x)}[\log D(x)] + \mathbb{E}_{z\sim P_z(z)}[\log(1 - D(G(z)))] \tag{8}$$

In Formula (8), $\mathbb{E}$ represents mathematical expectation. $x \sim P_{\text{data}}(x)$ represents randomly extracting real data from a real data set. $D(x)$ represents the discriminant score of the discriminator for real data x. $D(G(z))$ represents the discriminator's discrimination score for false data $G(z)$. The loss function of the generator is shown in Formula (9).

$$\min_G V(D,G) = \mathbb{E}_{z\sim P_z(z)}[\log(1 - D(G(z)))] \tag{9}$$

In Formula (9), $z \sim P_z(z)$ represents false data extracted from the generator data set. The generator improves the quality of generated samples by minimizing the discrimination probability. The discriminator improves its accuracy by maximizing its ability to distinguish real samples and generate samples. The final GAN function is shown in Formula (10).

$$\max_D \min_G V(D,G) = \mathbb{E}_{x\sim P_{\text{data}}(x)}[\log D(x)] + \mathbb{E}_{z\sim P_z(z)}[\log(1 - D(G(z)))] \tag{10}$$

In Formula (10), the generator and discriminator gradually reach a dynamic equilibrium point during the training process. The generator can generate false samples that are close to real samples. Discriminators have also become increasingly difficult to distinguish the real samples and generated samples. GAN is applied to generate back texture. Then a back texture generation algorithm based on GAN is constructed. The structure of this algorithm is shown in Figure 5.

In Figure 5, the input human frontal texture image is segmented to obtain the binary mask of the image. Subsequently, the human frontal texture and binary mask are input into the data generator to output the predicted human back texture. The output human back texture is shown in Formula (11).

$$\hat{I}_b = G(I_f, S_f) \tag{11}$$

In Formula (11), I_f represents the frontal texture image of the human body. S_f represents a binary mask for human body images. G represents the generator. To ensure the correct matching between the generated back texture image and the input front texture image, the input of the discriminator in back texture generation algorithm is a set of images. The back texture $\hat{I}_b$ and front texture image I_f of the human body are used as

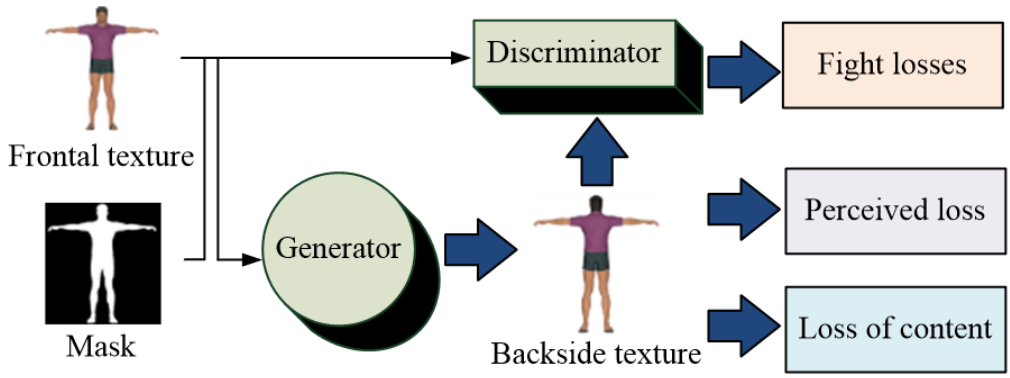

Figure 5. Schematic diagram of the back texture generation algorithm based on GAN.

inputs. A discriminator is used to rate the inputs. A high score indicates high authenticity. The loss function of the back texture generation algorithm based on GAN is shown in Formula (12).

$$LOSS = \lambda_{GG} L_{VGG} + \lambda_{pix} L_{pix} + \min_{G} \max_{D} L_{GAN}(D, G) \tag{12}$$

In Formula (12), λ_{GG} represents the perceived loss coefficient. L_{VGG} represents image perception loss. λ_{pix} represents the pixel loss coefficient. L_{pix} represents pixel loss in the image. The pixel difference between images is shown in Formula (13).

$$L_{pix} = \left\| \hat{I}_b - I_b \right\|_{l_1} \tag{13}$$

In Formula (13), I_b is the real back texture image. $\hat{I}_b$ represents the predicted back texture image generated by the generator. The perceptual loss between images is shown in Formula (14).

$$L_{VGG} = \left\| f(\hat{I}_b) - f(I_b) \right\|_{l_1} \tag{14}$$

In Formula (14), $f(\hat{I}_b)$ represents the feature tensor of the generated predicted back texture image. $f(I_b)$ represents the feature tensor of the real back texture image.

$$L_{GAN}(D, G) = \mathbb{C}_{I_f, I_b}[\log D(I_f, I_b)] + \mathbb{C}_{I_f, S_f}[\log(1 - D(I_f, G(I_f, S_f)))] \tag{15}$$

After completing the human back texture generation based on GAN, human animation is synthesized using motion data and 3D human models. The synthesis method of this animation is shown in Figure 6.

In Figure 6, the frontal image of the human body is taken as input. It is used to construct a human mask image. Subsequently, the human posture, morphology, and expression parameters are extracted. A 3D model of the human body with both sides is constructed based on SMPL-X. To maintain the smoothness and naturalness of the model, a fusion algorithm based on the cubic B-spline difference model is designed. The geometric model of the hand is replaced and the front and back models are concatenated. Subsequently, the model refinement is carried out. A human back texture generation algorithm based on GAN is constructed. This algorithm is applied to the 3D model of the human body to construct a human body parameterized model with complete textures.

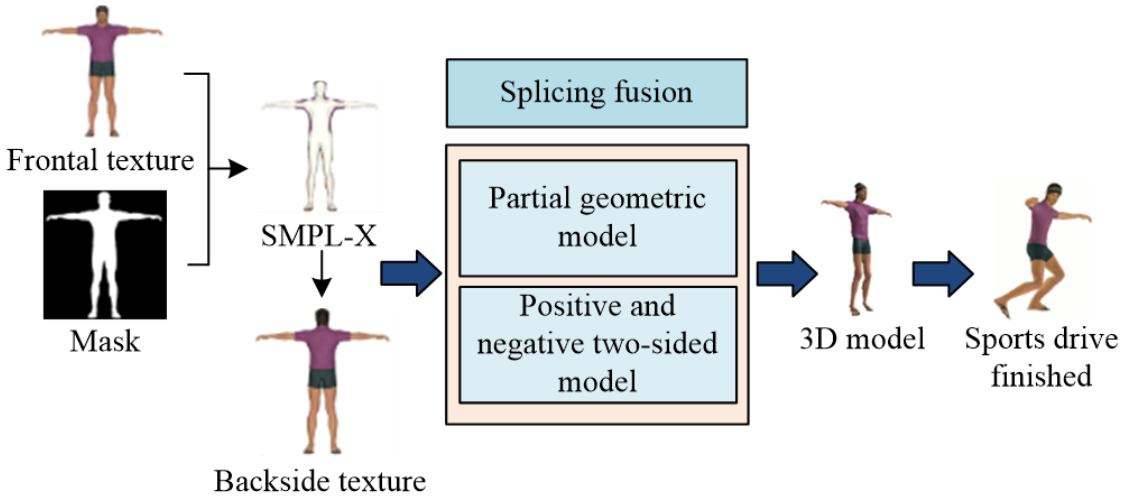

Figure 6. 3D model synthesis of the human body and synthesis of the human body animation

Finally, the 3D animation synthesis of the human body is executed. Based on the motion database, pose parameters are extracted. Motion-driven design is used to complete animation action design. Finally, the generated human animation is rendered.

3. An empirical study on the synthesis of 3D human animation.

3.1. Effectiveness analysis of model splicing and fusion algorithms based on B-Spline difference.

The model stitching and fusion algorithm based on B-spline difference and the GAN back texture generation algorithm are tested for performance verification. An empirical analysis is conducted to verify the feasibility of the 3D human animation synthesis method that combines B-spline difference and GAN.

To verify the effectiveness of the proposed model stitching and fusion algorithm based on B-spline differences, this algorithm is used in smooth curve trajectory fitting experiments with traditional stitching fusion algorithms, T-spline based stitching fusion algorithms, and C-spline based stitching fusion algorithms. By simulating the trajectory of the third-order Bessel curve, various comparison stitching fusion algorithms are verified for smoothness. The comparison indicators are fitting error, fitting time, and fitting compression rate. The experimental environment is a Windows 10 64 bit operating system. The experimental platform is Matlab 2017. The programming languages are C++ and OpenGL. The fitting error of each comparison splicing fusion algorithm is shown in Figure 7.

Figure 7(a) shows the fitting error of traditional stitching fusion algorithms. In Figure 7(a), the maximum fitting error of traditional stitching fusion algorithms is 10.0*10-4. The average fitting error is 7.8*10-4. Figure 7(b) shows the fitting error of the stitching fusion algorithm based on T-spline difference. In Figure 7(b), the maximum fitting error of the stitching and fusion algorithm is 10.0*10-4. The average fitting error is 5.4*10-4. Figure 7(c) shows the fitting error of the stitching fusion algorithm based on C-spline difference. In Figure 7(c), the maximum fitting error of the stitching fusion algorithm is 10.0*10-4. The average fitting error is 5.8*10-4. Figure 7(d) shows the fitting error of the stitching fusion algorithm based on the cubic B-spline difference. In Figure 7(d), the maximum fitting error of the stitching and fusion algorithm is 10.0*10-4. The average fitting error is 4.6*10-4. The average fitting error is 3.2*10-4 lower than the traditional splice fusion algorithm, 0.8*10-4 smaller than the T-spline fusion algorithm, and 1.2*10-4

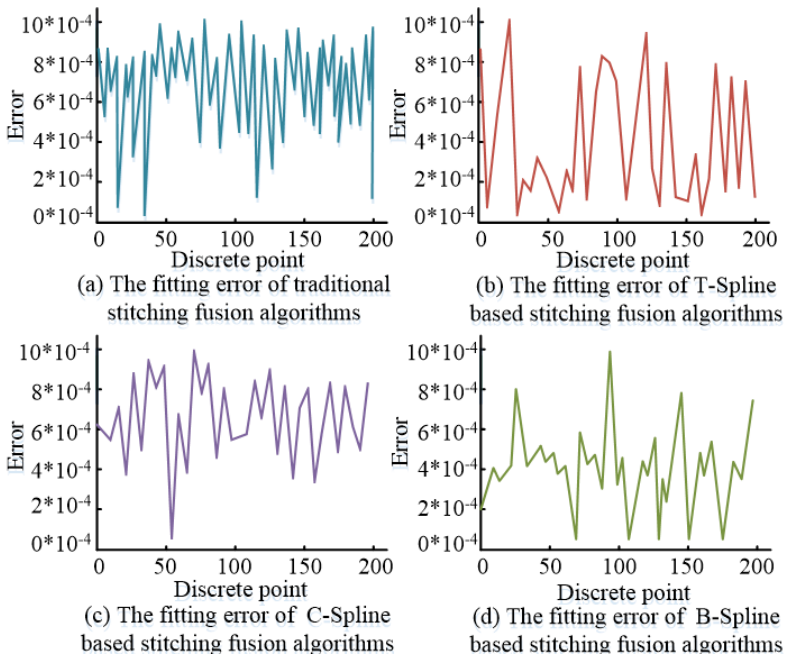

Figure 7. Comparison of the fitting error results for each splicing and fusion algorithm

less than the splice algorithm based on T-spline. Based on the above results, the proposed stitching fusion algorithm based on cubic B-spline difference has the smallest error. The fitting compression ratio and fitting time of each comparative fusion algorithm are shown in Figure 8.

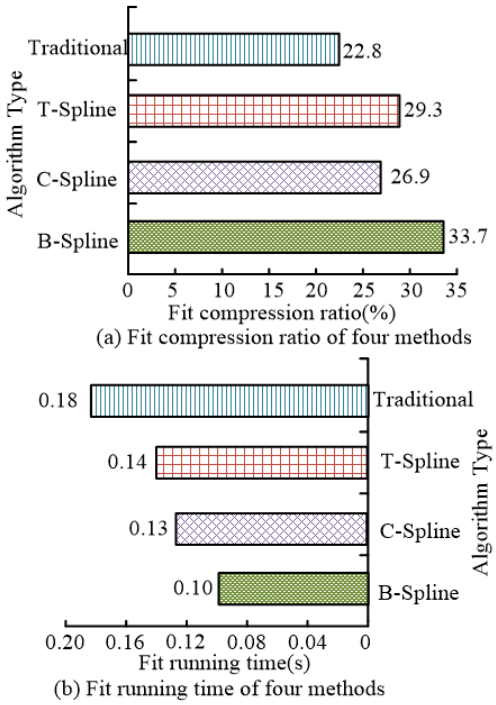

Figure 8. Fitting compression rate and fitting time of each comparative splicing fusion algorithm

Figure 8(a) shows the compression rate of each comparative stitching fusion algorithm. In Figure 8(a), the proposed fitting compression rate based on B-spline difference is higher than other algorithms, reaching 33%. The fitting efficiency is the best. Figure 8(b) shows the fitting time of each comparative stitching fusion algorithm. In Figure 8(b), the proposed fitting time based on B-spline difference is shorter than other algorithms, with a fitting time of 0.10s. It is 0.08s shorter than traditional splicing fusion algorithm, 0.04s shorter than T-spline based algorithms, and 0.03s shorter than T-spline based splicing fusion method. The fitting time is minimal. Based on the above results, the proposed stitching fusion algorithm based on B-spline difference has better fitting performance, which can complete model fitting better and faster.

3.2. **Performance verification experiment of GAN back texture generation algorithm.** To verify the effectiveness of the proposed GAN based back texture generation algorithm, performance comparison experiments are conducted on the algorithm. The comparison algorithms are based on Variational Auto-encoder (VAE), PixelCNN, and auto-encoder based back texture generation algorithms. PSNR, Structural Similarity Index (SSIM), Mean Square Error (MSE), and Visual Information Fidelity (VIF) are used to quantitatively evaluate the correlation between the back and front texture images generated by each algorithm. The data set used in the experiment is the Impersonator data set. The experimental environment is Intel(R) Xeon(R) Silver 4210. The experimental platform is Ubuntu 18.04 LTS. The programming language is Python 3.6. The PRSN and SSIM values of each back texture generation algorithm are shown in Figure 9.

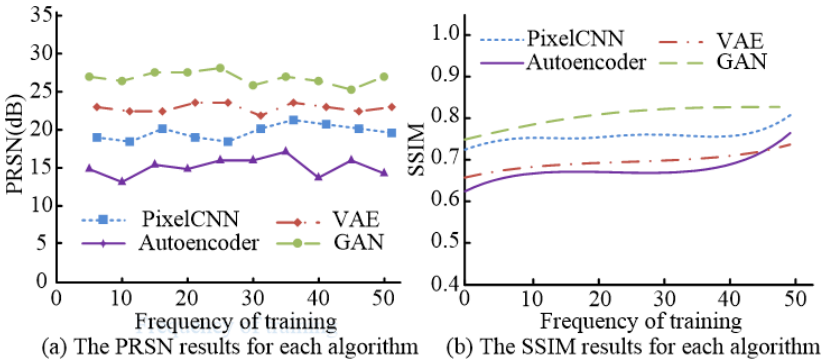

Figure 9. Comparison results of PRSN and SSIM values of each back texture generation algorithm

Figure 9(a) shows the PRSN comparison results of various back texture generation algorithms. In Figure 9(a), the proposed back texture generation algorithm based on GAN has a PRSN value of 25.6dB, which is 1.8dB higher than the back texture generation algorithm based on VAG. Compared to the PixelCNN based back texture generation algorithm, the PRSN is 4.8dB higher. Compared to the back texture generation algorithm based on auto-encoder, the PRSN is 9.6dB higher. The quality of the generated images is higher than the comparison algorithms. Figure 9(b) shows the SSIM comparison results of various back texture generation algorithms. In Figure 9(b), the proposed back texture generation algorithm based on GAN has a SSIM value of 0.84. Compared to the back texture generation algorithm based on VAG, the SSIM is 0.15dB higher. Compared to the back texture generation algorithm based on PixelCNN, the SSIM is 0.1dB higher. It is 0.17dB higher than the back texture generation algorithm based on the auto-encoder. The similarity between the generated back texture image and the front texture is higher than other comparison algorithms. Based on the above results, the proposed back texture

generation algorithm based on GAN has better image quality performance. The MSE and VIF results of each comparison algorithm are shown in Figure 10.

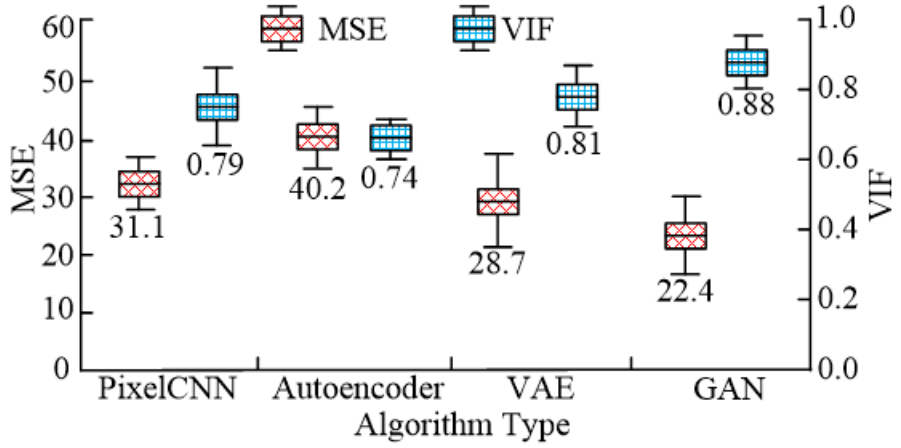

Figure 10. MSE and VIF comparison results of each back texture generation algorithm

In Figure 10, the MSE value of the proposed back texture generation algorithm based on GAN is 22.4, which is lower than other comparison algorithms. It indicates that the proposed method has the smallest error. The accuracy of matching with the front texture is higher. In addition, the VIF value of this algorithm is also higher than other comparative algorithms, reaching 0.88. The quality of generated images is higher. Based on the above results, compared to other algorithms, the proposed back texture generation algorithm based on GAN generates back texture images with higher matching accuracy. The generated images also have better quality and practical value.

3.3. **Performance comparison experiment of 3D human animation synthesis.** To verify the feasibility of the proposed 3D human animation synthesis method based on B-spline difference and GAN back texture generation algorithm, a corresponding 3D human animation is generated using human action posture video and a random action video. The matching accuracy, error rate, animation synthesis time, and expert satisfaction of generated animations are used for performance comparison experiments. The comparison methods are the Grassmann Manifold method [22] and the HSOM method [23]. The data set used is the UTKinect Action3D data set, which includes 10 different action categories. Six of these actions are selected as test subjects for the study. Firstly, the performance verification of the proposed 3D animation generation method is conducted. The confusion matrix of action matching results in the 3D animation generation results is shown in Figure 11.

In Figure 11, in the action matching of the proposed 3D human animation generation method, the rows of the confusion matrix represent the actual action categories. The lists represent the action categories that generate the animation. In diagonal elements, the values on the diagonal of this matrix are higher than 0.87. The values on non diagonal lines not exceed 0.04. This indicates that the method generates the correct matching angles for animation actions, which meets the requirements for correct matching of 3D animation actions. Subsequently, the accuracy and error performance of action matching for different animation generation methods are compared. The accuracy and error results of action matching for each 3D animation generation method are shown in Figure 12.

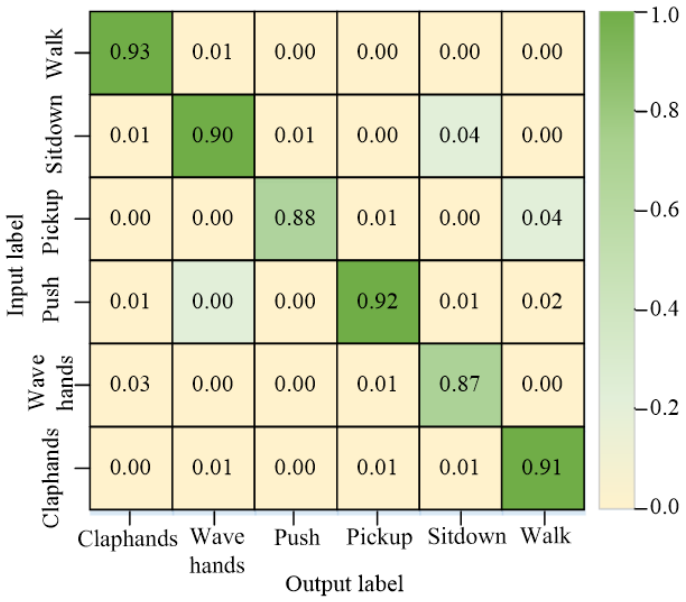

Figure 11. Confusion matrix of action-matching results

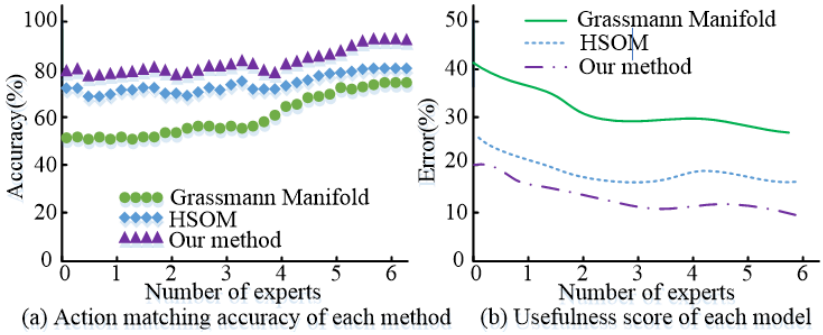

Figure 12. Action matching accuracy and error comparison results of each 3-dimensional animation generation method

Figure 12(a) shows the action matching accuracy of various 3D animation generation methods. In Figure 12(a), the proposed 3D human animation synthesis method based on B-spline difference and GAN has an action matching accuracy of 87.8%. Compared to the Grassmann Manifold method, it is 9.4% higher. Compared to the HSOM method, it is 7.2% higher. The proposed method has the best accuracy performance. Figure 12(b) shows the action matching error rate results of each 3D animation generation method. In Figure 12(b), the proposed 3D human animation synthesis method based on B-spline difference and GAN has an action matching error rate of 12.2%. Compared to the Grassmann Manifold method, it is 9.4% lower. Compared to the HSOM method, it is 7.2% lower. The proposed method has the smallest error. Based on the above results, the proposed 3D human animation synthesis method based on B-spline difference and GAN outperforms the comparison methods in action matching performance for outputting animations. The generated 3D animation has high quality.

4. **Conclusion.** In recent years, the quality requirements for 3D human animation have become increasingly high in society. To further improve the details and action accuracy of

3D human animation design, an improved human model reconstruction algorithm is constructed based on B-spline difference. A back texture generation algorithm is constructed based on GAN. Based on this, a fusion 3D human animation design method is designed. Empirical analysis is conducted on the two improved algorithms proposed in the study. The average fitting error of the human model reconstruction algorithm is 4.6*10-4, which is 3.2*10-4 lower than the traditional splicing-fusion algorithm. Compared with T-spline fusion algorithm, it is 0.8*10-4 lower. Compared with the splice algorithm based on T-spline, it is 1.2*10-4 lower. The fitting compression rate is 33%, and the fitting time is 0.10 s, which is 0.08s shorter than the traditional splice fusion algorithm, 0.04s shorter than the T spline fusion algorithm, and 0.03s shorter than the the splice algorithm based on T-spline. The PSNR of the proposed back texture generation algorithm based on GAN is 25.6dB. The PRSN is 1.8dB higher than the back texture generation algorithm based on VAG, 4.8dB higher than the PRSN based on the back texture generation algorithm of PixelCNN, and 9.6dB higher than the PRSN based on the back texture generation algorithm based on the auto-encoder. The quality of the generated images is higher than the comparison algorithms. The structural similarity is 0.84. The SSIM is 0.15 higher than the VAG based back texture generation algorithm, 0.1dB higher than the back texture generation algorithm based on PixelCNN, and 0.17 higher than the back texture generation algorithm based on the auto-encoder. In addition, empirical analysis is conducted on the designed 3D human animation. The values on the diagonal of the action confusion matrix are all higher than 0.87. The accuracy of action matching is 87.8%, which is 9.4% higher than the Grassmann Manifold method and 7.2% higher than the HSOM method. Based on the above results, the proposed fusion method for 3D human animation has better detail quality and action matching than other methods, solving the unreality of human form and unnatural motion in 3D human animation design. It has great potential in practical applications. But the research also has certain shortcomings. During the reconstruction of the proposed human model, some non frontal and anti human texture details are missing. In the future, the algorithm for generating back texture will be further optimized to improve the detail quality and realism of 3D human models

Fundings. The research is supported by Jiangsu Province Qinglan Project: Jiangsu Province University Philosophy and Social Science Research Project (2023SIYB1329).

REFERENCES

[1] B. Wang, R. Santoreneos, L. Giles, H.-A.-A. Hossein, and H. Marshall, "Case fatality rates of invasive meningococcal disease by serogroup and age: A systematic review and meta-analysis," *SSRN Electronic Journal*, vol. 37, no. 21, pp. 2768-2782, 2019.

[2] A. Chen, and P.-D.-B. Harrington, "Self-optimizing support vector elastic net," *Analytical Chemistry*, vol. 92, no. 23, pp. 15306-15316, 2020.

[3] W. Gan, L. Chen, S. Wan, J. Chen, and C.-M. Chen, "Anomaly rule detection in sequence data," *IEEE Transactions on Knowledge and Data Engineering*, vol. 35, no. 12, pp. 12095-12108, 2023.

[4] K. Wang, M. Zhu, W. Boulila, M. Driss, T.-R. Gadekallu, C.-M. Chen, L. Wang, S. Kumari, and S.-M. Yiu, "SeqNovo: De novo peptide sequencing prediction in IoMT via Seq2Seq," *IEEE Journal of Biomedical and Health Informatics*, vol. 4, pp. 1-11, 2023.

[5] S. Yniesta, and M. Janati-Idrissi, "Integration of Viscoplastic Effects in a one-dimensional constitutive model for ground response analysis," *Canadian Geotechnical Journal*, vol. 58, no. 4, pp. 468-478, 2020.

[6] Y. Fang, B. Luo, and T. Zhao, "ST-SIGMA: Spatio-temporal semantics and interaction graph aggregation for multi-agent perception and trajectory forecasting," *CAAI Transactions on Intelligence Technology*, vol. 7, no. 4, pp. 744-757, 2022.

[7] Z. Sun, Y. Gan, J. Tao, Z. Huang, and X. Zhou, "An improved quadrature scheme in B-spline material point method for large-deformation problem analysis," *Engineering Analysis with Boundary Elements*, vol. 138, pp. 301-318, 2022.

[8] R.-R. Hiemstra, T.-J. Hughes, C. Manni, H. Speleers, and D. Toshniwal, "A Tchebycheffian extension of multi-degree B-splines: Algorithmic computation and properties," *SIAM Journal on Numerical Analysis*, vol. 58, no. 2, pp. 1138-1163, 2020.

[9] Y. Zhu, X. Zhang, and K. Yuan, "Medical image super-resolution using a generative adversarial network," *IET Image Processing*, vol. 13, no. 14, pp. 2673-2679, 2019.

[10] H. Chen, R. Chen, and N. Li, "Attentive generative adversarial network for removing thin cloud from a single remote sensing image," *IET Image Processing*, vol. 15, no. 4, pp. 856-867, 2021.

[11] M.-M. Aristov, H. Geng, A. Pavelic, and J.-F. Berry, "A new library of 3D models and problems for teaching crystallographic symmetry generated through Blender for use with 3D printers or Sketchfab," *Journal of Applied Crystallography*, vol. 55, no. 1, pp. 172-179, 2022.

[12] Y. Ishida, T. Kumamoto, H. Watanabe, Y. Kurahashi, and H. Shinohara, "Creation of virtual three-dimensional animation using computer graphic technology for videoscopic transcervical upper mediastinal esophageal dissection," *Journal of Laparoendoscopic and Advanced Surgical Techniques*, vol. 30, no. 3, pp. 304-307, 2019.

[13] S. Long, S. Andreopoulos, S. Patterson, J. Jenkinson, and D.-P. Ng, "Metabolism in motion: Engaging biochemistry students with animation," *Journal of Chemical Education*, vol. 98, no. 5, pp. 1795-1800, 2021.

[14] M. Dvoroňák, D. Skora, C. Curtis, B. Curless, O. Sorkine-Hornung, and D. Salesin, "Monster mash: a single-view approach to casual 3D modeling and animation," *ACM Transactions on Graphics*, vol. 39, no. 6, pp. 1-12, 2020.

[15] S. Sebastian, H. Norman, and Z. Jianwei, "Memetic evolution for generic full-body inverse kinematics in robotics and animation," *IEEE Transactions on Evolutionary Computation*, vol. 23, no. 3, pp. 406-420, 2018.

[16] J. Zhou, M. Campen, D. Zorin, C. Tu, and C.-T. Silva, "Quadrangulation of non-rigid objects using deformation metrics," *Computer Aided Geometric Design*, vol. 62, no. 3, pp. 3-15, 2018.

[17] C.-S. Jreige, R.-N. Kimura, A.-R.-T.-C. Segundo, C. Coachman, and N. Sesma, "Esthetic treatment planning with digital animation of the smile dynamics: A technique to create a 4-dimensional virtual patient," *The Journal of Prosthetic Dentistry*, vol. 128, no. 2, pp. 130-138, 2021.

[18] J. Singla, K. Burdsall, B. Cantrell, J.-R. Halsey, A. Mcdowell, and C. Mcgregor, "A new visual design language for biological structures in a cell," *Structure*, no. 4, pp. 485-502, 2022.

[19] F. Zhang, T.-Y. Wu, J.-S. Pan, G. Ding, and Z. Li, "Human motion recognition based on SVM in VR art media interaction environment," *Human-Centric Computing and Information Sciences*, vol. 9, no. 40, pp. 1-15, 2019.

[20] F. Zhang, T.-Y. Wu, and G. Zheng, "Video salient region detection model based on wavelet transform and feature comparison," *EURASIP Journal on Image and Video Processing*, vol. 58, pp. 1-10, 2019.

[21] W. Gan, L. Chen, S. Wan, J. Chen, and C.-M. Chen, "Anomaly rule detection in sequence data," *IEEE Transactions on Knowledge and Data Engineering*, vol. 35, no. 12, pp. 12095-12108, 2012.

[22] M. Oulghelou, and C. Allery, "Non intrusive method for parametric model order reduction using abi-calibrated interpolation on the Grassmann manifold," *Journal of Computational Physics*, vol. 426, no. 1, pp. 1-26, 2021.

[23] M.-V.-B. Santana, C. Sansour, M. Hjiaj, and H. Somja, "An equilibrium-based formulation with nonlinear configuration dependent interpolation for geometrically exact 3D beams," *International Journal for Numerical Methods in Engineering*, vol. 123, no. 2, pp. 444-464, 2022.